JACS
JOURNAL OF THE AMERICAN CHEMICAL SOCIETY
Article
pubs.acs.org/JACS

Electron Flow through Nitrotyrosinate in *Pseudomonas aeruginosa* Azurin

Jeffrey J. Warren, Nadia Herrera, Michael G. Hill, Jay R. Winkler, and Harry B. Gray*

Beckman Institute and Division of Chemistry and Chemical Engineering, California Institute of Technology, Pasadena, California 91125, United States

Department of Chemistry, Occidental College, Los Angeles, California 90041, United States

Supporting Information

ABSTRACT: We have designed ruthenium-modified *Pseudomonas aeruginosa* azurins that incorporate 3-nitrotyrosine (NO_2YOH) between Ru(2,2′-bipyridine)$_2$(imidazole)(histidine) and Cu redox centers in electron transfer (ET) pathways. We investigated the structures and reactivities of three different systems: RuH107NO_2YOH109, RuH124NO_2YOH122, and RuH126NO_2YOH122. RuH107NO_2YOH109, unlabeled H124NO_2YOH122, and unlabeled H126NO_2YOH122 were structurally characterized. The pK_a's of NO_2YOH at positions 122 and 109 are 7.2 and 6.0, respectively. Reduction potentials of 3-nitrotyrosinate (NO_2YO^-)-modified azurins were estimated from cyclic and differential pulse voltammetry data: oxidation of NO_2YO^-122 occurs near 1.1 versus NHE; oxidation of NO_2YO^-109 is near 1.2 V. Our analysis of transient optical spectroscopic experiments indicates that hopping via NO_2YO^- enhances Cu^I oxidation rates over single-step ET by factors of 32 (RuH107NO_2YO^-109), 46 (RuH126NO_2YO^-122), and 13 (RuH124NO_2YO^-122).

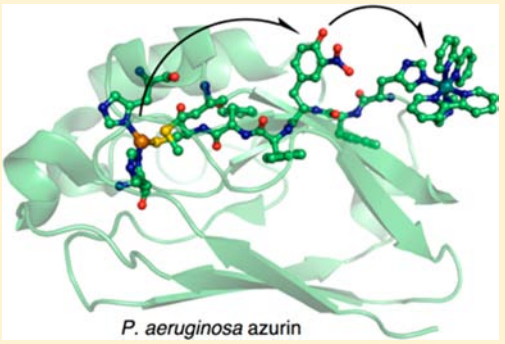

1. INTRODUCTION

Biological redox transformations rely on efficient electron/hole transport over long molecular distances (>10 Å). Key examples include water oxidation in photosystem II,[1] O_2 reduction in cytochrome *c* oxidase,[2] deoxynucleoside production in ribonucleotide reductases (RNR),[3] H^+/H_2 interconversion in hydrogenases,[4] and N_2 reduction in nitrogenases.[5] Single-step electron transfer (ET) cannot deliver electrons/holes in milliseconds or less to protein active sites over distances exceeding 20 Å, so many enzymes employ redox way stations to promote rapid multistep ET (hopping).[6] Understanding and incorporating these natural design elements into artificial redox systems to promote rapid electron/hole separation and long-lived charge separated states is of great interest for use in solar energy capture and conversion.

Our work on ET in Ru-modified metalloproteins, including *Pseudomonas aeruginosa* azurin,[7,8] has been informed by semiclassical ET theory[9,10] (eq 1, ss = single-step tunneling). Note that $1/\tau_{ss} = k_{ss}$, which is the sum of the forward and reverse rate constants for a single-step

$$\tau_{ss} = \frac{1}{\sqrt{\frac{4\pi^3}{h^2\lambda RT}}(H^0_{AB})^2 \exp(-\beta(r_1 - r_0))\left(\exp\left(\frac{-(\Delta G^\circ_{DA} + \lambda)^2}{4\lambda RT}\right) + \exp\left(\frac{-(\Delta G^\circ_{DA} - \lambda)^2}{4\lambda RT}\right)\right)} \quad (1)$$

ET reaction. Set out in Figure 1 are modified hopping maps[6,11] that show the predicted hopping advantage (with respect to single-step ET) for Ru-H107, Ru-H124, and Ru-H126 azurins with a generalized intermediate (Int) situated between a diimine-Ru^{III} oxidant and Cu^I. The maps compare the total ET times for hopping from a donor (D) to an intermediate (I) to an acceptor (A) (τ_{hop}, eq 2, hop = hopping) versus single-step D to A tunneling (τ_{ss})[12] (eq 1). As above, $1/\tau_{hop} = k_{hop}$, which is a function of all of the forward and reverse rate constants for ET between D, I, and A.[6a]

$$\tau_{hop} = \frac{\exp\left(\beta(r_2 - r_0) + \frac{(\Delta G^\circ_{IA} + \lambda)^2}{4\lambda RT}\right)\left(1 + \exp\left(\frac{\Delta G^\circ_{DI}}{RT}\right)\right) + \exp\left(\beta(r_1 - r_0) + \frac{(\Delta G^\circ_{DI} + \lambda)^2}{4\lambda RT}\right)\left(1 + \exp\left(\frac{\Delta G^\circ_{IA}}{RT}\right)\right)}{\sqrt{\frac{4\pi^3}{h^2\lambda RT}}(H^0_{AB})^2\left(1 + \exp\left(\frac{\Delta G^\circ_{IA}}{RT}\right) + \exp\left(\frac{\Delta G^\circ_{DA}}{RT}\right)\right)} \quad (2)$$

Maps were generated assuming a reorganization energy (λ) of 0.8 eV, an electronic coupling decay constant (β) of 1.1 Å^{-1}, and $H_{AB}{}^0$ (r_0 = 3 Å) of 186 cm^{-1} for each ET reaction.[7] Note that the maps are not symmetric. In all cases, the greatest hopping advantage occurs in systems where the Int-Ru^{III} distance (r_1) is up to 5 Å shorter than the Int-Cu^I distance (r_2). The hopping advantage increases as systems orient nearer a "straight-line" between the donor and acceptor (the black diagonal), which is a result of minimizing intermediate tunneling distances. The smallest predicted hopping advantage area is in Ru−H124 azurin, which has the shortest Ru−Cu distance of the three proteins.

The maps in Figure 1 illustrate how the hopping advantage at a fixed D−A distance changes as a function of driving force ($-\Delta G^\circ$). The hopping advantage is nearly lost as the driving force for the first step ($Ru^{III} \rightarrow$ Int) falls below −0.15 eV.

Received: April 15, 2013
Published: July 16, 2013

   dx.doi.org/10.1021/ja403734n | *J. Am. Chem. Soc.* 2013, 135, 11151−11158

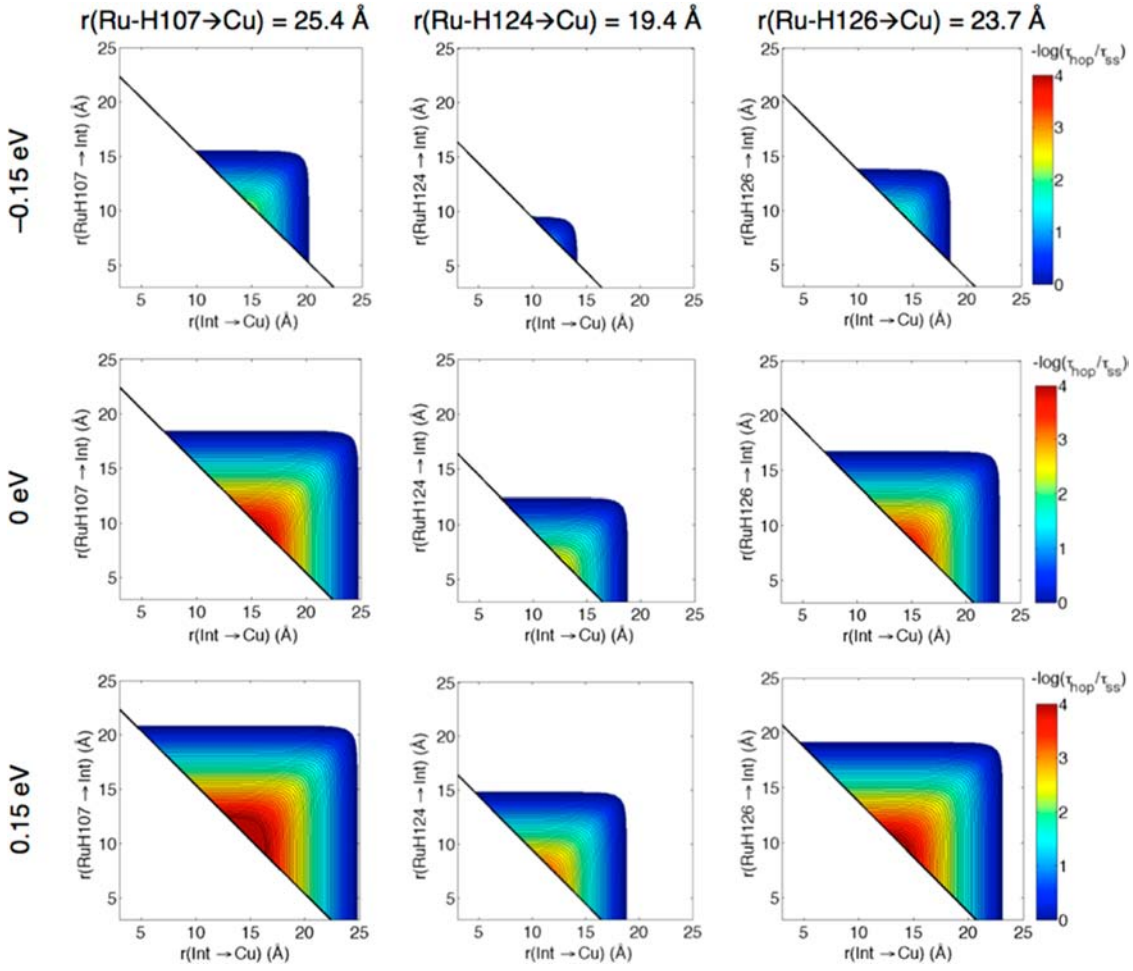

Figure 1. Hopping advantage maps for a two-step ET system ($Cu^{I} \rightarrow Int \rightarrow Ru^{III}$) in each of three azurins. In each map the overall driving force $-\Delta G^{o}(Cu^{I} \rightarrow Ru^{III})$ is 0.7 eV, the reorganization energy (λ) is 0.8 eV, T is 298 K, the distance decay constant (β) is 1.1 $Å^{-1}$, and the close-contact coupling element ($H_{AB}{}^{0}$) is 186 cm^{-1}. τ_{hop} is the calculated hopping rate constant and τ_{ss} is the calculated single-step rate constant. The first step driving forces ($-\Delta G^{o}(Int \rightarrow Ru^{III})$) are indicated at the left. The contour lines are plotted at 0.1 log unit intervals.

Isoergic initial steps provide a wide distribution of arrangements, where advantages as great as 10^4 are possible (for a fixed donor−acceptor distance of 23.7 or 25.4 Å). A slightly exergonic $Int \rightarrow Ru^{III}$ step provides an even larger distribution of arrangements for productive hopping, which will be the case as long as the driving force for the first step is not more favorable than that for overall transfer.

We have used nitrotyrosinate (NO_2YO^-) as a redox intermediate in three Ru-His labeled azurins to test the hopping advantage for net $Cu^{I} \rightarrow Ru^{III}$ ET. The phenol pK_a of 3-nitrotyrosine is 7.2,[13] allowing us to work at near-neutral pH, rather than high pH (>10) required to study analogous reactions in tyrosine. Investigating ET via nitrotyrosinate also avoids the complexities associated with the kinetics of proton-coupled redox reactions of tyrosine.[14] The NO_2YOH model compound *N*-acetyl-3-nitrotyrosinamide has pK_a similar to that of 3-nitrotyrosine and the $NO_2YO^{\bullet/-}$ reduction potential ($E^{o\prime} \approx 1.02$ V versus NHE) is similar to that[15] of $Trp^{\bullet+/0}$ and Ru-diimine photosensitizers.[16] It follows that hole transfer via NO_2YO^- can be described using semiclassical ET theory, because it is not a proton-coupled redox reaction.[14,17] We prepared three azurins with NO_2YO^- situated between the Ru and Cu sites: RuH107NO_2YOH109; RuH124NO_2YOH122; and RuH126NO_2YOH122. The first two systems have cofactor placements that are close to optimal; the last system has a larger first-step distance, which is predicted to decrease the hopping advantage.

RESULTS

2.1. Synthesis and Characterization. Site-directed mutants of *P. aeruginosa* azurin with surface-exposed Tyr residues were obtained using standard procedures,[18] and NO_2YOH was produced by reaction with tetranitromethane (TNM).[19] Our modified azurin has additional mutations (W48F/Y72F/H83Q/Y108F) such that only a single Tyr residue was available for TNM modification (M109Y or K122Y) and a single His residue for Ru-labeling (Q107H, T124H or T126H). Nitration of YOH was confirmed by mass spectrometry and UV−vis spectroscopy (see Supporting Information [SI]). At basic pH, NO_2YO^- exhibits a visible absorption maximum at 420 nm,[19] imparting a vivid green color to Cu^{II} proteins. Yields for TNM modification for each protein were ≥90% based on UV−vis quantification of protein following FPLC purification. The UV−vis spectra of all three of the NO_2YOH- or NO_2YO^--azurins were found to be the sum of the component spectra of azurin and free nitrotyrosine or nitrotyrosinate (see SI), thereby confirming that the

dx.doi.org/10.1021/ja403734n | J. Am. Chem. Soc. 2013, 135, 11151−11158

NO_2YO^-, Ru-label, and azurin-Cu are very weakly coupled in the modified protein.

Spectrophotometric titration of Cu^{II}–NO_2YOH azurins from pH 4 to pH 10 gave clean conversions to nitrotyrosinate (NO_2YO^-) (Figure 2). $NO_2YOH109$ has pK_a = 6.0 ± 0.05,

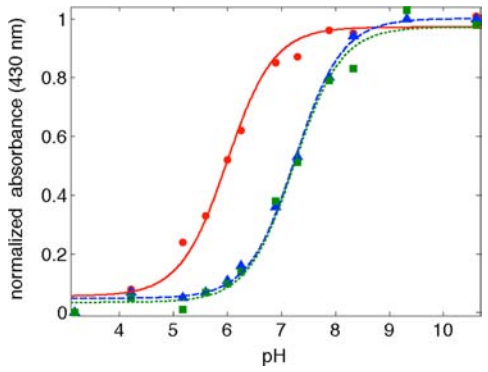

Figure 2. Titration curves for: H107$NO_2YOH109$ (red ●); H124$NO_2YOH122$ (green ■) and H126$NO_2YOH122$ (blue ▲). The lines are fits as described in Materials and Methods.

over 1 pK_a unit lower than nitrotyrosine models (7.2).[13,15] $NO_2YOH122$ (with His at either position 124 or 126) has pK_a = 7.2 ± 0.05. These pK_a's could be slightly shifted in the Ru-labeled proteins, but UV–vis spectra at pH > 8, as used in our time-resolved laser experiments, are consistent with complete conversion to NO_2YO^- (see SI).

The $NO_2YO^{\bullet/-}$ reduction potentials were investigated using cyclic voltammetry (all reduction potentials are referenced to NHE). Measurements were problematic because the $NO_2YO^{\bullet/-}$ couple is near the solvent window (20 mV/s scan rate, 50 mM potassium phosphate, 50 mM KCl, pH 8.3, Figure 3). The azurin-$Cu^{II/I}$ couple ($E^{o\prime}$ = 0.30 ± 0.01 V[20]) remained

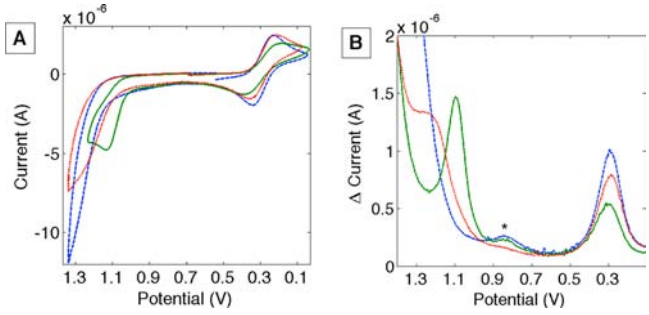

Figure 3. (A) Cyclic voltammograms (20 mV/s) of H124NO_2YO^-122 azurin (green –––), H107NO_2YO^-109 (red ●●●) and all Phe azurin (blue - - -). (B) Differential pulse voltammograms (DPVs) for H124NO_2YO^-122 azurin (green –––), H107NO_2YO^-109 (red ●●●), and all Phe azurin (blue - - -). The asterisk indicates a background wave. Potentials are versus NHE.

constant in all variants, providing a convenient internal standard. NO_2YO^-122 azurins exhibited an anodic wave at 0.8 V versus the Cu anodic wave (Figure 3A), consistent with E^o values for NO_2YO^- model compounds.[15] Unfortunately, an analogous oxidative wave was not observed for NO_2YO^-109 azurin. A modest increase in anodic current above 1 V compared to "all Phe" azurin (where all Tyr/Trp residues are replaced with Phe) can be seen in the voltammogram of NO_2YO^-109 azurin.

We turned to differential pulse voltammetry (DPV) in an effort to better resolve the electrochemical response attributed to oxidation of nitrotyrosinate.[21] DPVs of 1 mM NO_2YOH-modified proteins in 50 mM potassium phosphate, 50 mM KCl exhibited a peak at 1.1 V for NO_2YO^-122 azurin and a shoulder at ~1.2 V for NO_2YO^-109 azurin. All Phe azurins exhibited a steeply increasing background signal, but no maxima or inflection points. As for CV experiments, $E^{o\prime}(Cu^{II/I})$ exhibited a peak at 0.30 ± 0.01 V.

$Ru^{II}(bpy)_2(im)$ labeling (bpy = 2,2′-bipyridine, im = imidazole) and purification of all three azurins were as described previously.[8,22] Successful labeling was confirmed by UV–vis spectroscopy and mass spectrometry. X-ray-quality crystals of Ru–H107$NO_2YOH109$-azurin were grown using sitting drop vapor diffusion.[23] Crystals of $NO_2YOH122$-azurin (without Ru at H124 or H126) also were obtained employing sitting drop vapor diffusion; however, the analogous Ru-labeled protein did not form crystals, even after several different crystallization experiments. Structures for each of the proteins that highlight the linkage between the Ru-labeling site and azurin-Cu are shown in Figure 4. Crystallographic details are given in Table 1. The distances shown in Figure 4 are those between Ru^{II} and NO_2YO^--C4; NO_2YO^--C4 and Cu^{II}; and Ru^{II} and Cu^{II} (r_1, r_2, and r_T, respectively). Justification of ET distances for mutants crystallized without Ru-labels is given in the SI.

2.2. Electron Transfer Reactivity. Electron transfer kinetics were investigated using time-resolved laser spectroscopy, with excitation at 500 nm (where NO_2YO^- absorbance is negligible). In the absence of exogenous electron acceptors, $*Ru^{II}(bpy)_2(im)(HisX)$ (X = 107, 124, 126) has a lifetime >300 ns. Oxidation of Cu^I-azurin by *Ru was not observed, consistent with previous findings.[7,8] $Ru^{III}(bpy)_2(im)(HisX)Cu^I$-azurin was generated using the flash-quench technique with 12 mM $[Ru(NH_3)_6]Cl_3$ as oxidative quencher. A bleach of $Ru^{II}(bpy)_2(im)(HisX)$ absorption at 480 nm was consistent with production of $Ru^{III}(bpy)_2(im)(HisX)$. Azurin-$Cu^{II}$ could be quantitatively recovered upon addition of $K_3Fe(CN)_6$ after laser experiments.

Oxidation of Cu^I to Cu^{II} in all three variants was monitored at 630 nm and the transients fit to a biphasic kinetics model; the first rate constant corresponds to decay of $*Ru^{II}$ and the second to intramolecular oxidation of Cu^I by Ru^{III} (Figure 5). Observed rate constants (k_{hop}) for Cu^I oxidation are set out in Table 2. The rate constants were independent of protein concentration between 18 and 60 μM in all cases. The state of the Ru complex was monitored at 480 nm: transient kinetics followed a double exponential function with the same rate constants found in the 630 nm traces. In all cases the fitting residuals were <5% of the total signal amplitude.

3. DISCUSSION

3.1. Structural and Thermodynamics Analyses. The X-ray structures of $Ru^{II}(bpy)_2(im)$H107NO_2YO^-109, H124$NO_2YOH122$ and H126$NO_2YOH122$ azurins are similar to those of other modified and unmodified azurins.[23,24] Electron density corresponding to the presence of NO_2YOH was observed in all three variants. The H124$NO_2YOH122$ and H126$NO_2YOH122$ crystals are blue, indicating that the nitrotyrosine residues are protonated, although the crystallization experiment was performed at pH = pK_a($NO_2YOH122$) where a 50/50 mixture of protonated and deprotonated species is expected. For $Ru^{II}(bpy)_2$(imidazole)(H107)$NO_2YOH109$

dx.doi.org/10.1021/ja403734n | J. Am. Chem. Soc. 2013, 135, 11151–11158

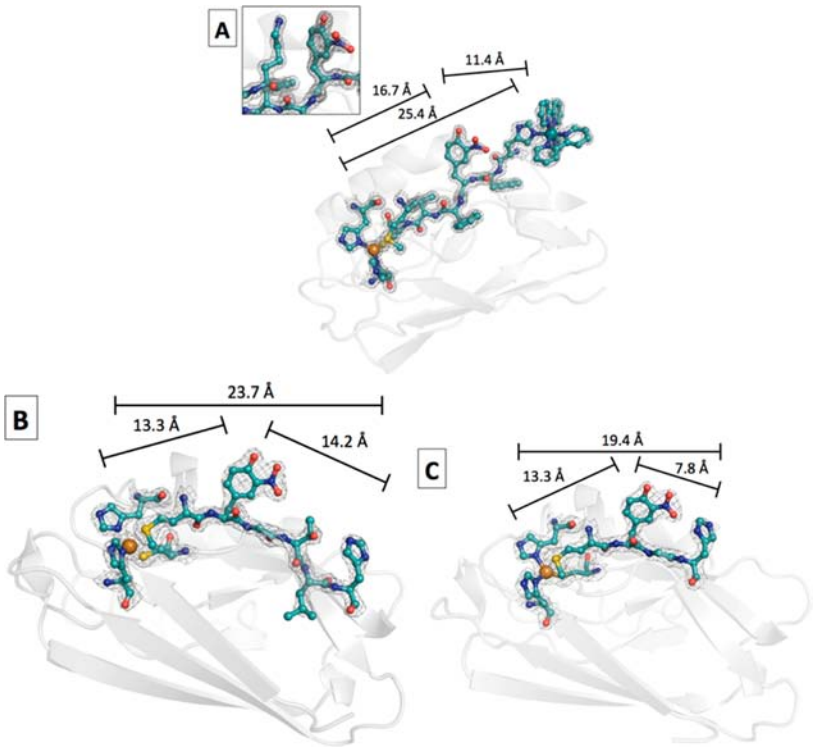

Figure 4. Structures of the electron transfer units of RuH107NO_2YO$^-$109 (PDB 4HHG, 1.6 Å) (A); H126NO_2YOH122 (PDB 4HIP, 1.9 Å) (B), and H124NO_2YOH122 (PDB 4HHW, 2.0 Å) (C) azurins. The peptide chain connecting the Ru-label, NO_2YOH, and azurin-Cu is shown in cyan, and the rest of the protein is shown as a gray ribbon. The distances between redox centers (see text) are shown above the black bars; the bars are not intended to show angles between cofactors. The inset in (A) shows Lys122. The Lys122(N) to NO_2YO($O_{phenolate}$) distance is 4.3 Å. Cu^{II} is depicted as an orange sphere, and Ru^{II} in (A) is a turquoise sphere.

Table 1. Crystallographic Statistics

	RuH107NO_2YOH109	H124NO_2YOH122	H126NO_2YOH122
PDB ID	4HHG	4HHW	4HIP
space group	*I*222	$P22_12_1$	$P22_12_1$
A, *B*, *C* (Å)	49.762, 67.176, 81.385	49.669, 65.637, 72.561	49.546, 65.804, 73.005
α, β, γ (deg)	90, 90, 90	90, 90, 90	90, 90, 90
observed reflections	255277	71623	82347
unique reflections	43899	16724	16630
completeness[a]	98.92% (99.02%)	98.42% (99.67%)	98.99% (99.77%)
R_{sym}[b]	12.3%	4.3%	4.2%
$I/\sigma I$[c]	5.1	21.6	22.6
resolution range (Å)	1.60−51.81	2.0−49.67	1.90−49.55
R_{free} (esu)	27.1% (0.112 Å)	28.1% (0.237 Å)	31.6% (0.203 Å)
$R_{working\ set}$ (esu)	23.5% (0.112 Å)	22.4% (0.207 Å)	25.0% (0.213 Å)
mean *B*	20.740	28.711	36.115
RMS deviation: bond lengths	0.022	0.021	0.015
RMS deviation: bond angles	2.439	1.913	1.862

[a]Total (outer shell). [b](SUM(ABS($I(h,i) - I(h)$)))/(SUM($I(h,i)$)). [c]Mean of intensity/σI of unique reflections (after merging symmetry-related observations).

azurin, the pH of the crystallization experiment (7.2) would suggest that the nitrotyrosine in (pK_a = 6.0) is largely deprotonated, but all Ru-labeled Cu^{II}-azurins are green, so the crystal color is not a reliable indicator of the nitrotyrosine protonation state. Inspection of the structure (Figure 4A) reveals that NO_2YO$^-$109 is in an environment that is distinct from that of NO_2YOH122. First, NO_2YO$^-$109 is about 4.3 Å from Lys122 (ammonium−nitrogen to phenolate−oxygen distance). Second, an oxygen atom in the nitro group of NO_2YO$^-$109 is near (2.9 Å) the side-chain oxygen of Thr124 (not shown in Figure 4A). Finally, the nitro group is rotated 38° out of the plane of the phenolate. In contrast to NO_2YO$^-$109, no substantial H-bonding or electrostatic interactions are apparent in the vicinity of NO_2YOH122. The orientations of the NO_2YOH122 aromatic ring and its nitro group are not affected by the presence of His at position 124 versus 126.

The H124NO_2YOH122 and H126NO_2YOH122 variants show an anodic voltammetric wave at ∼1.1 V (pH 8.3) and pK_a = 7.2; values that closely parallel those of related small

dx.doi.org/10.1021/ja403734n | J. Am. Chem. Soc. 2013, 135, 11151−11158

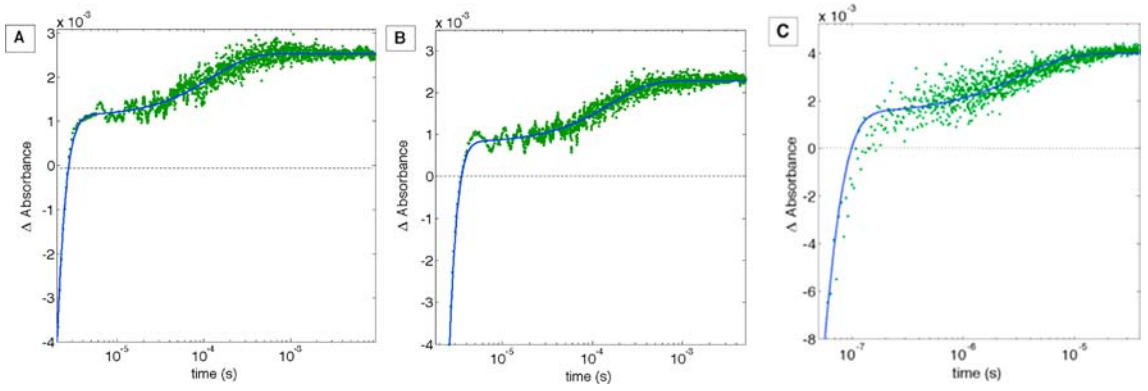

Figure 5. Transient absorption traces (630 nm) for RuH107NO_2YO$^-$109 (A), RuH126NO_2YO$^-$122 (B), and RuH124NO_2YO$^-$122 (C) azurins. Kinetics traces were fit as described in the experimental section. The apparent bleach at very early times is due to residual luminescence from *Ru. The concentration of $Ru(NH_3)_6Cl_3$ was 12 mM in each sample.

Table 2. Electron Transfer Rate Constants for Nitrotyrosine-Modified Azurins

	k_{hop}	$k_{hop(calc)}$ [a]	k_{ss} [c]	k_{hop}/k_{ss}
Ru(H107)	$(7.7 \pm 0.5) \times 10^3$	8.7×10^2 [b]	$(2.4 \pm 0.5) \times 10^2$ [d]	32 ± 7
Ru(H126)	$(6.0 \pm 0.5) \times 10^3$	2.3×10^3	$(1.3 \pm 0.6) \times 10^2$ [e]	46 ± 22
Ru(H124)	$(3.0 \pm 0.5) \times 10^5$	1.3×10^6	$(2.2 \pm 0.2) \times 10^4$ [e]	14 ± 3

[a] $k_{hop(calc)}$ are from the hopping maps shown in Figure 6. [b] Calculated with $\Delta G°(NO_2YO^-109 \rightarrow Ru^{III}) = 0.2$ eV. [c] $k_{ss} = k_{single\text{-}step}$ for Ru(bpy)$_2$imidazole(HisX)-labeled wild-type azurin. [d] Reference 8b. [e] Reference 8c.

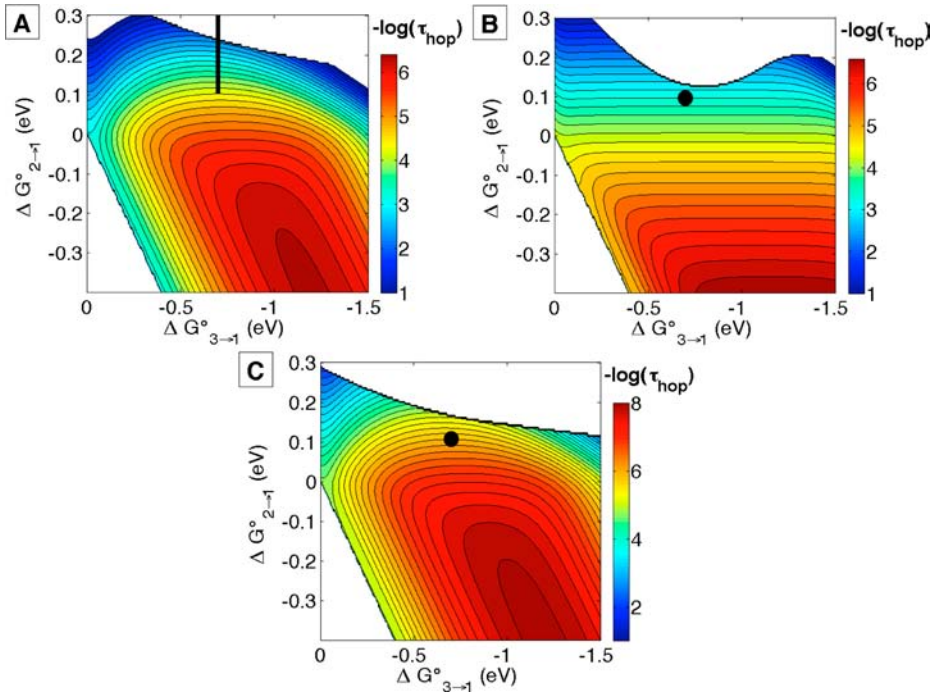

Figure 6. Hopping maps for NO_2YO^--substituted azurins: (A) RuH107NO_2YO$^-$109 with $r_1 = 11.4$, $r_2 = 16.7$, $r_T = 25.4$ Å. (B) RuH126NO_2YO$^-$122 with $r_1 = 14.2$, $r_2 = 13.3$, $r_T = 23.7$ Å. (C) RuH124NO_2YO$^-$122 with $r_1 = 7.8$, $r_2 = 13.3$, $r_T = 19.4$ Å (Figure 4). In all maps $\lambda = 0.8$ eV, $\beta = 1.1$ Å^{-1}, $T = 298$ K, and $H_{AB}{}^0 = 186$ cm^{-1}. The subscripts 1, 2, and 3 refer to Ru^{III}, NO_2YO^-, and Cu^I respectively. The contour lines are plotted at 0.2 log unit intervals. The black dots (or black bar in (A)) are at the driving forces given in the text. The calculated rate constants are set out in Table 2.

molecules.[15] Given the surface exposure and neutral electrostatic protein environment around NO_2YOH122, the similarity to model complexes is reasonable. On the other hand, NO_2YOH109 has a lower pK_a (6.0), and anodically scanned differential pulse voltammograms exhibit a shoulder at ~1.2 V. Electrostatic interaction with Lys122, as well as the interaction of the nitro group with Thr124, could contribute to those apparent shifts. The influence of the nitro torsional angle on $E°$ and pK_a has not been reported. An internal H-bond between a nitro oxygen and the phenolic proton in 2-nitrophenol hinders rotation,[25] potentially explaining the difference in torsional angle in H107NO_2YO$^-$109 versus the other two NO_2YOH-modified azurins. While pK_a perturbation of NO_2YOH residues is a useful tool for characterizing protein active sites,[26] such

dx.doi.org/10.1021/ja403734n | J. Am. Chem. Soc. 2013, 135, 11151−11158

perturbations arise from the interplay of many factors and do not provide any quantitative insight into the $NO_2YO^{\bullet/-}109$ reduction potential.

3.2. Electron Transfer Reactivity. Detailed analysis of electron flow in the three NO_2YO^--modified azurins requires reasonable estimates of reduction potentials, distances between cofactors, reorganization energies, and electronic couplings. The $Ru^{III/II}(bpy)_2(im)_2$ reduction potential is assumed to be the same as that in the labeled proteins without NO_2YOH residues ($E^o \approx 1.0$ V[16]). We take E^o(azurin-$Cu^{II/I}$) = 0.3 V,[20] and use our CV/DPV data to estimate $E^o(NO_2YO^{\bullet/-}122)$ = 1.10 ± 0.05 V, and $E^o(NO_2YO^{\bullet/-}109)$ = 1.2 ± 0.1 V (Figure 3). We assume that Ru-photosensitizers do not dramatically alter the nitrotyrosine redox properties, which is reasonable because the sites are very weakly coupled (based on the close agreement between observed and the linear combination of component UV−vis spectra, see SI).

The Ru−Cu and Ru−NO_2YOH distances for the $H107NO_2YOH109$ protein were taken directly from the X-ray coordinates (Figure 4A). We used structures of related rhenium-labeled azurins[24] to estimate the Ru−Cu distances in the $RuH124NO_2YOH$ and $RuH126NO_2YOH$ proteins (see SI). We used a center-to-center distance formulation in our analysis, but the corresponding analysis for edge-to-edge distances also is given in the SI. This distance formulation does not affect the main conclusions.

The maps in Figure 6 are calculated with $H_{AB}{}^0$ = 186 cm^{-1}, β = 1.1 $Å^{-1}$, and λ = 0.8 eV, the same as for our investigation of single-step ET in closely related azurins.[8] As in those models, the Ru-label, NO_2YO^- residue, and a Cu-ligating residue (Cys112 or Met121) also are oriented on a single β strand (Figure 4). The sites are probably coupled similarly in the single-step and hopping systems, so β = 1.1 $Å^{-1}$ is a reasonable starting point for our analysis. Likewise, the value for λ was validated for single-step ET in Ru-modified wild-type azurins.[7,8] A λ near 0.8 eV is able to account for the rate of bimolecular phenoxyl/phenolate electron self-exchange in basic water,[27] as well as other similarly sized organic molecules,[28] so use of our empirical λ is reasonable here. Additional hopping maps are presented in the SI that illustrate how subtle changes in ET distances, β, and λ can affect the shape of hopping maps and the predicted tunneling times.

Specific rates of Cu^I oxidation (Table 2) are more than 10 times greater than those of single-step ET in the corresponding azurins lacking NO_2YOH (107 or 122), confirming that NO_2YO^- accelerates long-range ET. We have shown that hopping maps can be used to estimate reaction times for generation of a product state in a three-site ET chain.[6] Using the above reduction potentials and structural data, we constructed hopping maps to gain insight into NO_2YO^--meditated intraprotein ET (Figure 6). In this case the proposed reaction sequence is [Ru^{III}-NO_2YO^--Cu^{II}] → [Ru^{II}-$NO_2YO^{\bullet}$-Cu^{I}] → [Ru^{II}-NO_2YO^--Cu^{II}], although the nitrotyrosyl radical intermediate was not detected by transient spectroscopy in any of the proteins investigated. Note that two-step hopping is a biphasic process, but the observed kinetics will appear single exponential under certain limiting conditions.[29]

The hopping maps predict electron transport times that are in good agreement with the experimentally determined rate constants (Table 2). Small fluctuations in driving forces, reorganization energies, and/or electronic couplings can affect the rate constants in hopping maps (see SI), but the predictions are still in accord with our experimental results. The experimental results also are consistent with the maps in Figure 1 (with $-\Delta G^o$ = −0.1 eV for the intermediate step) as expected, given that the maps are a product of semiclassical theory. Overall, we find that a 100−200 meV endergonic intermediate redox step with NO_2YO^- accelerates long-range ET by more than 10-fold.

3.3. Multistep Electron Transfer. The azurin-based hopping models described here provide structural data and thermodynamics estimates that can be used to analyze the design criteria taken from semiclassical ET theory (Figure 1). The driving forces do not vary widely, but the structural variations among model systems allow for analysis of the spatial factors that are central to functional hopping. Further, these model hopping systems employ a well characterized ground state oxidant, in contrast to previous investigations where electronically excited Re^I was used as the electron acceptor.[24] These reactions, involving ground or electronically excited electron acceptors, are models for biological hopping: the Ru-NO_2YO^- systems mimic ground state hopping in enzymes such as RNR (though ET there is proton-coupled[3a]), while the electronically excited Re systems mimic phototriggered hopping in proteins such as PS II.[1]

Although Trp-promoted Cu^I oxidation in Re-azurin was enhanced 100-fold,[24a] rates in the three NO_2YO^--modified Ru-proteins increased by factors of just 10−50. This finding is attributable to differences in the driving force for the first step: for the Re-azurins it is near zero; for the Ru-proteins it is ≤−0.1 eV. We predict that rate enhancements of up to 10^4 are possible with the appropriate driving forces and arrangement of redox sites (Figures 1 and 6). The first step becomes rate limiting when the distance between the donor and intermediate is large, giving the hopping map a "ladder" appearance, and a parabolic boundary where single-step ET is favored at $-\Delta G_{31}{}^o \approx \lambda$ and $\Delta G_{21}{}^o > 0.1$ eV (Figure 6).

The basic shape of each hopping map is unique (Figure 6), although each of these shapes could change with variations in ET parameters (see SI). The driving force ranges where hopping is predicted to be favored over single-step tunneling depend strongly on the distances between cofactors and the reorganization energies. The arrangement of cofactors that gives the widest range is that in which the redox intermediate is (spatially) closer to the start of the ET chain (e.g., $RuH107NO_2YO^-109$ and $RuH124NO_2YO^-122$). All else being equal, such systems are predicted to have the greatest hopping advantages (Figure 1). When the intermediate is closer to the ultimate electron/hole acceptor, the driving force associated with the first step effectively limits the ET rates. Native biological electron transport systems rarely employ the latter arrangement; the ones we have analyzed[6] appear to have evolved cofactor arrangements that efficiently control electron or hole delivery as required for function.

Interestingly, $RuH126NO_2YO^-$ azurin exhibits the greatest hopping advantage, with nonoptimal arrangement in which the first ET step occurs over a longer distance than the second. Modeling suggests that hopping is possible in such systems, but the energetic landscape is much different (Figures 1 and 6). We can rationalize the reactivity of $RuH126NO_2YO^-$ azurin by distinguishing between the hopping advantage and the absolute hopping rate constant. Figure 1 illustrates that the maximum predicted hopping advantage increases as the total donor−acceptor distance increases (Figure 1, top row, 10^1 for 19.4 Å versus $10^{2.5}$ for 25.7 Å). This finding is a result of the exponential distance dependence of ET reactions: breaking up a

dx.doi.org/10.1021/ja403734n | J. Am. Chem. Soc. 2013, 135, 11151−11158

longer distance into shorter two steps has a greater impact than breaking up a shorter distance. Conversely, hopping systems with the shortest overall distances (e.g., 19.4 Å for RuH124NO_2YO^-122 azurin) cannot attain high hopping advantages, but produce the largest absolute rate constants by dividing a shorter ET distance into two steps of less than 10 Å. RuH107NO_2YO^-109 azurin has a hopping advantage slightly smaller than that for RuH126NO_2YO^-122 azurin, contradicting the predictions in Figure 1, but advantages gained by favorable cofactor arrangement can be offset by small changes in driving force, reorganization, and/or electronic coupling pathways (see SI). Semiclassical theory provides important guidelines for designing hopping systems, but hopping advantages must be determined by experiment.

4. CONCLUSIONS

Efficient multistep electron transport requires careful redox cofactor arrangement and finely tuned reaction driving forces. We have shown that multistep ET between azurin-Cu^I and Ru^{III} is enhanced over single-step reactions in three Ru-labeled azurins, providing an experimental demonstration of the interplay between driving force and cofactor arrangement in defining the hopping advantage. Semiclassical ET theory provides the insights needed to design systems that rapidly separate electrons and holes and, importantly, maintain that separation on long time scales.

5. MATERIALS AND METHODS

Buffer salts were obtained from J.T. Baker. Tetranitromethane and imidazole were from Sigma-Aldrich. Terrific broth was from BD Biosciences. Solutions were prepared using 18 MΩ-cm water, unless otherwise noted. Ru(2,2′-bipyridine)$_2Cl_2$ and $[Ru(NH_3)_6]Cl_3$ were from Strem Chemicals. $Ru(NH_3)_6Cl_3$ was recrystallized prior to use.[30] Mass spectrometry was performed in the Caltech Protein/Peptide MicroAnalytical Laboratory (PPMAL).[31] UV−visible spectra were recorded on an Agilent 8453 diode array spectrophotometer. All data were collected at ambient temperature (~293 K).

Plasmids encoding for mutant azurins were generated using the Stratagene Quikchange protocol. Proteins were expressed[18] and tyrosine residues were nitrated[19] using known protocols. Purity was assessed using UV−vis and mass spectrometry.

The pK_a's of nitrotyrosine residues were determined by adding aliquots of a concentrated azurin solution (in water, pH 7) to 100 mM phosphate-citrate buffer (pH 3−10) and measuring the optical spectra of the resulting solutions. Data at 430 nm were fit using eq 3. Extinction coefficients (ε_{430}) for $NO_2YO(H)$ were determined by comparison to the known values for azurin (ε_{630} = 5700 M^{-1} cm^{-1}).[32] The ε_{430} were close to those for model complexes (4300 M^{-1} cm^{-1}).[15] The pK_a values were independent of protein concentration between 10 and 60 μM. Clean isosbestic points in the UV−vis spectra for each titration are consistent with the mass balance assumption implicit in eq 3.

$$A_{430} = \frac{\varepsilon(NO_2YO^-)\cdot 10^{(pH-pK_a)} + \varepsilon(NO_2YOH)}{1 + 10^{(pH-pK_a)}} \quad (3)$$

Electrochemistry was carried out using a standard three-electrode setup: homemade basal-plane graphite (www.graphitestore.com) working electrode;[33] Ag/AgCl reference electrode; Pt wire counter electrode. The working electrode was gently abraded with 600 grit wet/dry sandpaper and polished with 1 μM alumina power on a microcloth polishing pad for 30 s between each scan. For all voltammetry experiments, protein solutions were 1 mM in 50 mM potassium phosphate buffer (pH 8.3) + 50 mM KCl. CVs were collected at a scan rate of 20 mV/s. DPVs were collected with the following parameters: pulse amplitude = 30 mV; pulse width = 100 ms; pulse period = 200 ms; sample width = 15 ms, increment = 2 mV. The potential of the observed waves was independent of concentration between 0.4 and 1 mM for each protein. Potentials were converted to NHE by adding 0.193 V.

X-ray-quality crystals of NO_2YOH-modifed azurin-Cu^{II} azurin were obtained as described previously.[23] Azurin (~20 mg/mL in 40 mM imidazole + 2 mM NaCl, pH 7.2) was mixed with an equivalent volume of well solution containing 26−34% of poly(ethylene glycol) (PEG) 4000, 100 mM lithium nitrate, 6.25 mM copper sulfate and 100 mM imidazole, pH 7.2. The drops were equilibrated versus 1 mL of well solution. All experiments were incubated at room temperature and crystals were observed after 3 days. Diffraction data were collected at the Stanford Synchrotron Radiation Laboratory (SSRL) beamline 12-2. The structures were solved by molecular replacement and then refined to the resolution limit from scaling/merging statistics. The coordinates of the structures have been deposited in the Protein Data Bank (Table 1).

All transient spectroscopic measurements were conducted in the Beckman Institute Laser Resource Center at Caltech. Excitation (500 nm) was provided by an optical parametric oscillator (Spectra-Physics, Quanta-Ray MOPO-700) pumped by the third-harmonic of a Q-switched Nd:YAG laser (Spectra-Physics, Quanta-Ray PRO-Series, 8 ns pulse width), as described elsewhere.[34] Note that the signal amplifier used in Figure 4A,B (ms time scales) is different from that in Figure 4C (μs time scales). Kinetics traces were collected at 630 and 480 nm for each protein sample. Protein samples were reduced using sodium ascorbate and desalted using PD-10 columns into 50 mM sodium phosphate + 50 mM NaCl (pH 8.0). The samples were deoxygenated by repeated pump−backfill cycles and left under an argon atmosphere for data collection. Data were fit using a function that takes into consideration signal from residual luminescence, as well as absorbance changes corresponding to the ET reaction of interest (eq 4). The first rate constant corresponds to decay of electronically excited Ru^{II}, and the second corresponds to intramolecular electron transfer from Cu^I to Ru^{III}.

$$\Delta OD_{apparent}(630\ nm) = C\cdot\log[A\cdot\exp(-k_1\cdot t) + 10^{(B\cdot\exp(-k_2\cdot t))}] \quad (4)$$

■ ASSOCIATED CONTENT

Supporting Information

Detailed protocols for tyrosine modification and ruthenium-labeling reactions, MS and UV−vis characterization, electron transfer distance determination in unlabeled proteins, additional hopping maps with variable λ and β parameters. This material is available free of charge via the Internet at http://pubs.acs.org.

■ AUTHOR INFORMATION

Corresponding Author

hbgray@caltech.edu

Notes

The authors declare no competing financial interest.

■ ACKNOWLEDGMENTS

Our work was supported by NIH (DK019038 to H.B.G. and J.R.W.; GM095037 to J.J.W.), an NSF Center for Chemical Innovation (Powering the Planet, CHE-0947829), and the Arnold and Mabel Beckman Foundation. We also acknowledge the Gordon and Betty Moore Foundation and the Sanofi-Aventis Bioengineering Research Program for their support of the Molecular Observatory facilities at the California Institute of Technology. X-ray crystallography data was collected at the Stanford Synchrotron Radiation Lightsource (SSRL), a Directorate of the SLAC National Accelerator Laboratory and an Office of Science User Facility operated for the U.S. Department of Energy, Office of Molecular Biology Program

and Environmental Research, and by the National Institutes of Health, National Center for Research Resources, Biomedical Technology Program (P41RR001209), and the National Institute of General Medical Sciences.

REFERENCES

(1) (a) Rappaport, F.; Diner, B. A. *Coord. Chem. Rev.* **2008**, *252*, 259−272. (b) McEvoy, J. P.; Brudvig, G. W. *Chem. Rev.* **2006**, *106*, 4455−4483. (c) Siegbahn, P. E. M. *Dalton Trans.* **2009**, *45*, 10063−10068.

(2) (a) Kaila, V. R. I.; Verkhovsky, M. I.; Wikström, M. *Chem. Rev.* **2010**, *110*, 7062−7081. (b) Brzezinski, P.; Aedelroth, P. *Curr. Opin. Struct. Biol.* **2006**, *16*, 465−472. (c) Hosler, J. P.; Ferguson-Miller, S.; Mills, D. A. *Annu. Rev. Biochem.* **2006**, *75*, 165−187.

(3) (a) Stubbe, J.; Nocera, D. G.; Yee, C. S.; Chang, M. C. Y. *Chem. Rev.* **2003**, *103*, 2167−2201. (b) Jiang, W.; Saleh, L.; Barr, E. W.; Xie, J.; Gardner, M. M.; Krebs, C.; Bollinger, J. M. *Biochemistry* **2008**, *47*, 8477−8484. (c) Yokoyama, K.; Smith, A. A.; Corzilius, B.; Griffin, R. G.; Stubbe, J. *J. Am. Chem. Soc.* **2011**, *133*, 18420−18432.

(4) (a) Mulder, D. W.; Shepard, E. M.; Meuser, J. E.; Joshi, N.; King, P. W.; Posewitz, M. C.; Broderick, J. B.; Peters, J. W. *Structure* **2011**, *19*, 1038−1052. (b) Fontecilla-Camps, J. C.; Volbeda, A.; Cavazza, C.; Nicolet, Y. *Chem. Rev.* **2007**, *107*, 4273−4303.

(5) (a) Seefeldt, L. C.; Hoffman, B. M.; Dean, D. R. *Curr. Opin. Chem. Biol.* **2012**, *16*, 19−25. (b) Danyal, K.; Mayweather, D.; Dean, D. R.; Seefeldt, L. C.; Hoffman, B. M. *J. Am. Chem. Soc.* **2010**, *132*, 6894−6895.

(6) (a) Warren, J. J.; Ener, M. E.; Vlček, A., Jr.; Winkler, J. R.; Gray, H. B. *Coord. Chem. Rev.* **2012**, *256*, 2478−2487. (b) Warren, J. J.; Winkler, J. R.; Gray, H. B. *Coord. Chem. Rev.* **2013**, *257*, 165−170.

(7) (a) Gray, H. B.; Winkler, J. R. *Q. Rev. Biophys.* **2003**, *36*, 341−372. (b) Gray, H. B.; Winkler, J. R. *Biochim. Biophys. Acta* **2010**, *1797*, 1563−1572. (c) Gray, H. B.; Winkler, J. R. *Proc. Natl. Acad. Sci. U.S.A.* **2005**, *102*, 3534−3539.

(8) (a) Regan, J. J.; Di, B., A. J.; Langen, R.; Skov, L. K.; Winkler, J. R.; Gray, H. B.; Onuchic, J. N. *Chem. Biol.* **1995**, *2*, 489−496. (b) Langen, R.; Chang, I.-J.; Germanas, J. P.; Richards, J. H.; Winkler, J. R.; Gray, H. B. *Science* **1995**, *268*, 1733−1735. (c) Langen, R. Electron Transfer in Proteins: Theory and Experiment. Ph.D. Thesis, California Institute of Technology, Pasadena, CA, 1995.

(9) (a) Marcus, R. A.; Sutin, N. *Biochim. Biophys. Acta* **1985**, *811*, 265−322. (b) Barbara, P. F.; Meyer, T. J.; Ratner, M. A. *J. Phys. Chem.* **1996**, *100*, 13148−13168.

(10) (a) Curry, W. B.; Grabe, M. D.; Kurnikov, I. V.; Skourtis, S. S.; Beratan, D. N.; Regan, J. J.; Aquino, A. J. A.; Beroza, P.; Onuchic, J. N. *J. Bioenerg. Biomembr.* **1995**, *27*, 285−293. (b) Beratan, D. N.; Skourtis, S. S.; Balabin, I. A.; Balaeff, A.; Keinan, S.; Venkatramani, R.; Xiao, D. *Acc. Chem. Res.* **2009**, *42*, 1669−1678.

(11) The maps in Figure 1 are derived in the same way as those in ref 6a (variable driving forces and fixed distances), but here we fixed the driving forces and varied the distances between cofactors. MATLAB scripts for creating hopping maps are available at: http://www.bilrc.caltech.edu/webpage/47

(12) Derivations of eqs 1 and 2 are given in ref 6a.

(13) (a) Sokolovsky, M.; Riordan, J. F.; Vallee, B. L. *Biochem. Biophys. Res. Commun.* **1967**, *27*, 20−25. (b) Riordan, J. F.; Sokolovsky, M.; Vallee, B. L. *Biochemistry* **1967**, *6*, 358−361.

(14) (a) Song, N.; Stanbury, D. M. *Inorg. Chem.* **2008**, *47*, 11458−11460. (b) Costentin, C.; Louault, C.; Robert, M.; Savéant, J.-M. *Proc. Natl. Acad. Sci. U.S.A.* **2009**, *106*, 18143−18148. (c) Schrauben, J. N.; Cattaneo, M.; Day, T. C.; Tenderholt, A. L.; Mayer, J. M. *J. Am. Chem. Soc.* **2012**, *134*, 16635−16645.

(15) (a) Yee, C. S.; Seyedsayamdost, M. R.; Chang, M. C. Y.; Nocera, D. G.; Stubbe, J. *Biochemistry* **2003**, *42*, 14541−14552. (b) DeFelippis, M. R.; Murthy, C. P.; Broitman, F.; Weinraub, D.; Faraggi, M.; Klapper, M. H. *J. Phys. Chem.* **1991**, *95*, 3416−3419.

(16) (a) Di Bilio, A. J.; Hill, M. G.; Bonander, N.; Karlsson, B. G.; Villahermosa, R. M.; Malmström, B. G.; Winkler, J. R.; Gray, H. B. *J. Am. Chem. Soc.* **1997**, *119*, 9921−9922. (b) Mines, G. A.; Bjerrum, M. J.; Hill, M. G.; Casimiro, D. R.; Chang, I.-J.; Winkler, J. R.; Gray, H. B. *J. Am. Chem. Soc.* **1996**, *118*, 1961−1965.

(17) (a) Warren, J. J.; Tronic, T. A.; Mayer, J. M. *Chem. Rev.* **2010**, *110*, 6961−7001. (b) Warren, J. J.; Winkler, J. R.; Gray, H. B. *FEBS Lett.* **2012**, *586*, 596−602.

(18) Chang, T. K.; Iverson, S. A.; Rodrigues, C. G.; Kiser, C. N.; Lew, A. Y.; Germanas, J. P.; Richards, J. H. *Proc. Natl. Acad. Sci. U.S.A.* **1991**, *88*, 1325−1329.

(19) Lee, J. C.; Langen, R.; Hummel, P. A.; Gray, H. B.; Winkler, J. R. *Proc. Natl. Acad. Sci. U.S.A.* **2004**, *101*, 16466−16471.

(20) Gray, H. B.; Malmström, B. G.; Williams, R. J. P. *J. Biol. Inorg. Chem.* **2000**, *5*, 551−559.

(21) (a) Martínez-Rivera, M. C.; Berry, B. W.; Valentine, K. G.; Westerlund, K.; Hay, S.; Tommos, C. *J. Am. Chem. Soc.* **2011**, *133*, 17786−17795. (b) Berry, B. W.; Martínez-Rivera, M. C.; Tommos, C. *Proc. Natl. Acad. Sci. U.S.A.* **2012**, *109*, 9739−9743.

(22) Chang, I.-J.; Gray, H. B.; Winkler, J. R. *J. Am. Chem. Soc.* **1991**, *113*, 7056−7057.

(23) (a) Crane, B. R.; Di Bilio, A. J.; Winkler, J. R.; Gray, H. B. *J. Am. Chem. Soc.* **2001**, *123*, 11623−11631. (b) Faham, S.; Day, M. W.; Connick, W. B.; Crane, B. R.; Di, B.; Angel, J.; Schaefer, W. P.; Rees, D. C.; Gray, H. B. *Acta Crystallogr., Sect. D* **1999**, *55*, 379−385.

(24) (a) Shih, C.; Museth, A. K.; Abrahamsson, M.; Blanco-Rodriguez, A. M.; Di, B.; Angel, J.; Sudhamsu, J.; Crane, B. R.; Ronayne, K. L.; Towrie, M.; Vlcek, A., Jr.; Richards, J. H.; Winkler, J. R.; Gray, H. B. *Science* **2008**, *320*, 1760−1762. (b) Blanco-Rodríguez, A. M.; Busby, M.; Ronayne, K.; Towrie, M.; Gradinaru, C.; Sudhamsu, J.; Sykora, J.; Hof, M.; Zalis, S.; Bilio, A. J. D.; Crane, B. R.; Gray, H. B.; Vlcek, A., Jr. *J. Am. Chem. Soc.* **2009**, *131*, 11788−11800.

(25) Hargittai, I.; Borisenko, K. B. *J. Mol. Struct.* **1996**, *382*, 171−176.

(26) Yokoyama, K.; Uhlin, U.; Stubbe, J. *J. Am. Chem. Soc.* **2010**, *132*, 8385−8397.

(27) Schuler, R. H.; Neta, P.; Zemel, H.; Fessenden, R. W. *J. Am. Chem. Soc.* **1976**, *98*, 3825−3831.

(28) Analyses of ET reactions of several small organic molecules indicate reorganization energies less than 1 eV. See: Eberson, L. *Adv. Phys. Org. Chem.* **1982**, 79−185.

(29) Here, the total tunneling times can be roughly approximated by calculating the ET rates between Ru^{III} and NO_2YO^- using semiclassical theory (eq 1) and the ET parameters set out in Figure 6. Driving force optimized forward ET (Cu^I to $NO_2YO^\bullet$) is approximately 100 times faster than the first ET step from NO_2YO^- to Ru^{III}, which also is consistent with our inability to observe $NO_2YO^\bullet$ intermediates.

(30) Meyer, T. J.; Taube, H. *Inorg. Chem.* **1968**, *7*, 2369−2379.

(31) http://www.its.caltech.edu/~ppmal/

(32) Rosen, P.; Pecht, I. *Biochemistry* **1976**, *15*, 775−786.

(33) Blakemore, J. D.; Schley, N. D.; Balcells, D.; Hull, J. F.; Olack, G. W.; Incarvito, C. D.; Eisenstein, O.; Brudvig, G. W.; Crabtree, R. H. *J. Am. Chem. Soc.* **2010**, *132*, 16017−16029.

(34) Dempsey, J. L.; Winkler, J. R.; Gray, H. B. *J. Am. Chem. Soc.* **2009**, *132*, 1060−1065.